Dynamic Conditional Encoding and Feature Frequency Parsing in Diffusion Probabilistic Models for Diabetic Foot Ulcer Detection Using Thermographic Imaging

Kousar Nikhath A.[1*], Sireesha C.[2], Swapna M.[3], Vijayetha Thoday[4], and Esther Rani D.[5]
[1] VNR Vignana Jyothi Institute of Engienering and Technology, Vignana Jyothi Nagar, Pragathi Nagar, Nizampet, Hyderabad 500090, Telangana, India
[2] Vasavi College of Engineering, Ibrahimbagh, Hyderabad 500031, Telangana, India
[3] Stanley College of Engineering Technology for Women, Chapel Road, Abids, Hyderabad 500001, Telangana, India
[4] Mukesh Patel School of Technology, Management and Engineering, NMIMS, Mumbai, Maharashtra 400056, India
[5] SV College of Engineering, Karakambadi Road, Tirupati 517507, India
e-mail: kousarnikhath@vnrvjiet.in

Abstract. Diabetic patients' odds of survival can be significantly increased by early identification of diabetic foot ulcers (DFU) Thermography is utilised to identify changes in planter temperature because diabetic foot causes planter ulcers. This study uses publicly accessible thermographic imaging data from patients in the diabetes group as to ll as the control group. For DFU detection, both image-level and patch-level thermograms are used. The work suggests an optimizer-based Diffusion Probabilistic Segmentation model (Op-DPS) for DFU identification. The work suggests Dynamic Conditional Encoding, which creates state-adaptive conditions for every sampling step, to progress the step-wise regional attention in DPS for segmentation tasks. In moderate the detrimental impact of high-frequency noise components in this approach, to also suggest the Feature Frequency Parser (FF-Parser). The paper presents a Football Optimisation Algorithm (FbOA) that uses high dimensionality, nonlinearity, and many local optima to fine-tune the parameters of the suggested model. FbOA is based on the strategic balance between exploration and corruption that is seen in football gameplay. The proposed Op-DPS model achieved exceptional performance with a precision of 89.55%, recall of 85.53%, F_1 score of 87.50%, Intersection-over-Union (IoU) of 88.96%, and an overall accuracy of 99.27% on diabetic foot ulcer segmentation tasks. These results demonstrate significant improvements over existing methods, highlighting the model's capability for accurate and reliable DFU detection. In order to efficiently explore and take advantage of the solution space, the algorithm incorporates short passes, long passes, and positional modifications to replicate players' tactical placement and movement. Image-level, patch-level, and image–patch combination data are used to generate the findings.

Keywords: diabetic foot ulcer; diffusion probabilistic segmentation model; football optimization algorithm; patch level images; thermographic image data; dynamic conditional encoding.

Paper #9193 received 4 Dec 2024; revised manuscript received 10 Jan 2025; accepted for publication 22 Jan 2025; published online 26 Mar 2025. doi: 10.18287/JBPE25.11.010304.

1 Introduction

Amputations related to diabetic foot ulcers (DFUs) pose a global health and financial burden [1]. They make up 10% of the diabetic health services expenditure in the UK [2]. The UK would save more than £250 GBP million annually if DFU cases to be reduced by one-third [3]. In addition to the costs of diabetes, the projected cost of DFU in the United States is between $9 and $13 billion [4]. "More than half of all DFUs result in infection, and patients with diabetes have a lifetime risk of up to 34% [5]. DFU is thought to be a clinical indicator of a higher risk of death and amputation [6]. Diabetes mellitus (DM), which is brought on by the body's inability to produce enough insulin, produces persistently elevated blood glucose levels, or hyperglycemia [7]. Long-term uncontrolled diabetes can result in problems such retinopathy, nephropathy, and the development of Charcot feet, amputation, or even death [8]. Uncontrolled diabetes mellitus affects nerves; sensory diabetic neuropathy is a loss of sensation that results from damage to the nerves in the legs or feet. When neuropathy prevents a patient from feeling a cut or ache in his foot, the cut leads to infection and exacerbates the foot disease [9]. The decreased blood flow is the other circumstance. Low blood flow in the arms and legs is a symptom of peripheral vascular disease. Ulcers might form if the injury is not healing because of inadequate blood supply [10]. Individuals with diabetes are most likely to develop diabetic foot ulcers (DFUs); around 15% of individuals have this condition [11].

Problems with diabetic feet can be costly and negatively affect a person's quality of life. By doing an early risk assessment and examination of diabetic patients' foot health, this may often be avoided or significantly postponed [12]. Temperature may be important for that reason. Neuropathy, ischaemia, or infection can cause changes in the temperature of diabetics' plantar feet [13–14]. While the normal difference is usually less than 1 ºC, temperature disparities between the right and left feet of more than 2.2 ºC (4 F) are deemed abnormal [15]. By using a thermal-imaging camera, issues may be found early on, thus saving time and money. If the temperature is higher than absolute zero, infrared thermography can be used to provide a clear image of the thermal energy generated by the site under real-time monitoring [16]. A non-invasive, non-contact, quick, painless, and economical method of taking a patient's skin temperature is thermography. Temperature variations on human skin may be detected using this imaging method [17].

A qualified specialist must evaluate the thermogram in order to identify the ulcer. It can be difficult to find these specialists, especially in isolated places [18]. Consequently, the provision of an automatic DFU identification system has been the focus of several research investigations. While several of them took into account visible-band (RGB camera) pictures [19], only a small number of them used foot thermograms [20]. Diabetic foot thermogram pictures are taken into consideration for DFU identification in this investigation. Three levels of thermogram data are used in the tests for DFU recognition: image-level, patch-level, and a combination of image-patch thermogram data. Using transfer learning, an optimizer-based deep-learning model is used to identify the DFU feet. To observe that lesions and organs are frequently unclear and challenging to distinguish from the background in thermos picture segmentation tasks. To get correct findings in this situation, an adaptive calibration procedure is essential. In order to create the suggested model, to suggest using Dynamic Conditional Encoding instead of vanilla conditional DPS. The suggested model uses the picture to condition each stage of the iterative sampling process before learning the segmentation map. At each stage, to include the segmentation map of the current phase into the picture pre encoding to accomplish adaptive regional attention. In particular, to adopt a multi-scale approach to fuse the picture prior on the feature level with the current step segmentation mask. As a result, the reconstruction accuracy is increased and the condition characteristics are dynamically enhanced by the corrupted current-step mask. We propose to use the Feature Frequency Parser (FF-Parser) to filter the features in the Fourier space in order to remove high-frequency noise from the damaged mask. Every skip connection path uses FF-Parsers for multi-scale integration.

The remainder of the paper's details are as follows. The background information and relevant research are presented in Section 2, and the dataset and specifics of the suggested model are included in Section 3. Section 4 presents the findings and comments. Section 5 now includes the conclusion.

2 Related Works

In order to precisely identify ulcer areas in images of patients' feet, Sarmun et al. [21] suggested a deep learning-based approach. Using innovative model ensemble techniques including to highlighted the bounding box fusion (WBF), Soft-NMS, and non-maximum suppression (NMS), our method integrates predictions from state-of-the-art object recognition models. The results obtained from the many state-of-the-art model architectures used in this study are both improved and more generally applicable when they are used in concert with one another. With an impressive 12.4% improvement over the previous benchmark, our WBF-based technique utilising YOLOv8m and FRCNN-ResNet101 achieves a mAP score of 86.4% at the Intersection-over-Union (IoU) threshold of 0.5 on the DFUC2020 dataset. Our models have consistently outperformed the competition in qualitative analyses using the IEEE DataPort Diabetic Foot dataset, which is another dataset that to test externally. Finally, a new ensemble model for DFU detection was developed and tested in our study. Medical professionals benefit from early screening and an improved diagnosis process thanks to an AI-driven tool that increases sensitivity to potential DFU cases. While we acknowledge that false positives can happen, our study shows that by integrating

human medical knowledge with AI-based DFU management strategies, patient care can be improved.

Medical image analysis has been the primary focus of El-Kady et al. [22] in their efforts to improve the accuracy of DFU diagnosis. The famous ResNet50 model and a hybrid model combining ResNet50 with Generative Adversarial Networks to be tested. With an F_1-score of 0.75 and an average accuracy and precision of 0.76, the ResNet50 worked fantastically, yielding outstanding results. The hybrid model accomplished better than these metrics with an average F_1-Score, precision, and accuracy of 0.84. More precise and effective DFU detection in clinical settings is within reach, thanks to our study's contribution to medical image processing literature. An important step forward in the treatment and management of DFU has been the hybrid model's substantial increase in diagnostic accuracy.

Basiri et al. [23] has created a standardised framework for DFU data gathering by developing a case report form, a comprehensive dataset called Zivot that includes clinical feature breakdowns of the patient population, and a baseline for DFU identification using this dataset and a UNet architecture. Following this protocol, to create the Zivot dataset featuring 269 patients with active DFUs, 3700 RGB images of the DFUs with corresponding temperature and depth maps were collected. An efficient method for collecting uniform and clean datasets was demonstrated using a deep learning network for bounding box prediction that was constructed using the UNet architecture with EfficientNet as the feature extractor. The network was trained using the Zivot dataset, and the evaluation metrics shows to be promising results: a mAP segmentation metric of 0.79 and an F_1-score metric of 0.86. This study and the Zivot database lay the groundwork for additional research on holistic and multimodal methods of DFU.

In order to assess the interpretability of deep learning (DL) models that are driven by explainability, Biswas et al. [24] introduced the DFU XAI framework. The goal of DFU XAI is to build an open DL framework by evaluating five DL models (Xception, DenseNet121, ResNet50, InceptionV3, and MobileNetV2) with three state-of-the-art explanation methods: Grad-CAM, SHAP, and LIME-local interpretable model-agnostic explanations. Outperforming the other four models, ResNet50 achieved remarkable results with 98.75% accuracy, 99.2% precision, 97.6% recall, 98.4% F_1-score, and 98.5% AUC. Using the DFU dataset, it is able to differentiate between healthy feet and diabetic foot ulcers, and to localise diabetic foot ulcers to specific locations on diabetic feet. Using a heat map, the location of the ulcer can be accurately determined and appropriate treatment can be provided.

In their presentation of an automated system for detecting and categorising DFU, Almufadi et al. [25] rely on transfer learning. In most cases, two physically distinct states − ischaemic and infection − are used to classify DFU to evaluate the autonomous DFU detection performance of trained Deep Convolutional Neural Network (DCNN) models. Seven models are compared: EfficientNetB0, DenseNet121, ResNet101, VGG16, MobileNetV2, InceptionV3, and InceptionResNetV2. One other model that to propose, E-DFu-Net, is built on pre-existing architectures and can help decrease overfitting. Experimental results show that E-DFu-Net does an excellent job, correctly identifying ischaemia with 97% accuracy and infections with 92%. Practitioners may now more effectively detect DFU cases because to this advancement, which improves upon previous methods.

An approach to image segmentation analysis of DFU through the internet of things using the technique of virtual sensing for semantically similar objects was proposed by Thota et al. [26] for deeper image segmentation. This method takes into account four levels of range segmentation: region-based, edge-based, image-based, and computer-aided design-based range segmentation. To simplify the multimodal process for semantic segmentation, object co-segmentation is employed in this study. It is anticipated that this will lead to improved validity and reliability evaluations. The experimental results demonstrate that the proposed model can perform segmentation analysis more efficiently and with less error than the existing methods. Results on the multiple-image dataset show that DFU produces an average segmentation score of 90.85% and 89.03% in two types of labelled ratios, i.e., 25% and 30%, respectively, after DFU using virtual sensing. Compared to the prior best performance, this is an improvement of 10.91% and 12.22%. In actual DFU tests, our proposed method achieved a 59.1% improvement over existing deep segmentation-based approaches; in comparison, its average picture smart segmentation improvements are 15.06%, 23.94%, and 45.41%. Interobserver reliability on the positive test, namely the likelihood ratio test set with just 0.25 million parameters, is 73.9% when using the specified range-based segmentation at the pace of labelled data.

Das et al. [27] described a novel Convolutional Neural Network (CNN) architecture called HCNNet, which combines several hybridised blocks from inception, residual, and dense modules with appropriately placed Squeeze-and-Excitation (SE) blocks and intermediate transition layers. Training the proposed HCNNet multiple times with varied optimiser and learning rate settings maximises its performance. Its 0.999 area under the curve (AUC) for ischaemia detection is quite encouraging. The experimental results show that the proposed HCNNet outperforms the existing SOTA methods.

Dhar et al. [28] introduced FUSegNet, a new model for segmenting diabetic foot ulcers that uses the pre-trained EfficientNet-b7 as its foundation, to circumvent the issue of insufficient training data. An enhanced spatial and channel squeeze-and-excitation (scSE) module that merges additive and max-out scSE is called P-scSE, or parallel scSE. At the middle of each decoder stage, the module is fused, resulting in a new configuration. In order to avoid max-out scSE at the top

decoder stage − which has a limited number of feature mappings − a shorted P-scSE is built. A number of augmentations, including morphological, intensity-based, and geometric augmentations, are applied to the data before it is fed into the network. The proposed model is initially evaluated using a publicly accessible dataset pertaining to chronic wounds. Its data-based dice score of 92.70% is the greatest of any method that has been documented. The model outperforms earlier scSE-based U-Net models in most categories according to Pratt's Figure of merits (PFOM) evaluations, which evaluate the accuracy of edge localisation. The model is subsequently entered into the MICCAI 2021 FUSeg challenge, where it will compete against x-FUSegNet, a variation of FUSegNet. In the FUSeg Challenge, the model that averages the outputs produced by FUSegNet using 5-fold cross-validation − x-FUSegNet − topped the leaderboard with a dice score of 89.23%.

According to Biswas et al. [29], a novel multi-scale feature fusion network called FusionNet can accurately differentiate between healthy and DFU skin by utilising multiple pre-trained convolutional neural network (CNN) approaches. Six hundred and eighty-one training images, 672 validation images, and 211 testing images were generated using a database including 6963 skin images (3,574 normal and 3,389 ulcer) taken from various patients. Beginning with three image preprocessing techniques − motion blur estimation, median filter, and Gaussian filter − fuzzy, irrelevant, and noisy data was first eliminated. After that, DenseNet201, VGG19, and NASNetMobile − three pre-trained convolutional neural network (CNN) algorithms − are used to extract high-frequency features from the input images. In order to predict DFU, a meta-tuner module was then fed the most discriminative features. Statistically significant differences between FusionNet and other sub-networks are found using analysis of variance (ANOVA) and Friedman tests. Finally, three eXplainable Artificial Intelligence (XAI) algorithms − Grad-CAM, LIME, and SHAP − are integrated into FusionNet to better explainability and transparency. The classification results provided by the FusionNet classifier are exceptional, with an accuracy of 99.05%, recall of 98.18%, precision of 100%, AUC of 99.09, and F_1-score of 99.08%. The medical field could benefit from our proposed FusionNet since it can distinguish between DFU and healthy skin.

Zhao et al. [30] developed the Diabetic Foot Smart tool, an intelligent measurement tool for diabetic foot ulcers. In order to confirm its usefulness in assessing DFU, this study set out to quantify the ulcer area. The sizes of the ulcers on 150 DFU images are measured using three different assessment tools: the ruler method, the Smart APP software suite, and the gold standard application, Image J to compared the three approaches' measuring times and outcomes. To characterise the intra- and inter-rater reliability, the Pearson correlation coefficient, intra-group correlation coefficient, and coefficient of variation were used. The Image J program shows that the median ulcer size was 4.02 cm^2 and that the mean measurement duration was 66.37 ± 7.95 s. The ruler method, which had an average measuring time of 171.47 ± 46.43 s, shows that the median ulcer area was 5.14 cm^2. The median ulcer size was 3.70 cm^2, and the mean measurement duration was 38.25 ± 6.81 s, as reported by the APP software. Although there was no notable distinction between the APP and Image J software ($Z = 1.103$, $p > 0.05$), there were notable differences between the ruler technique and the industry standard Image J software ($Z = -4.123$, $p < 0.05$). Furthermore, with intra- and inter-rater reliability both reaching 0.99, the APP software proved to be quite reliable.

Finding consensus among stakeholders involved in DFU care about relevant and viable quality indicators (QIs) was the goal of Lusendi et al.'s study [31], which was the second part of a Belgian QI selection research that aimed to find QIs for DFU therapy. Stakeholders in diabetic foot care included a patient organisation representative and healthcare professionals from both primary care and speciality fields. Using the RAND/UCLA Appropriateness Method, stakeholders are asked to rate the appropriateness of 42 prospective evidence-based indicators on a 9-point Likert scale. To classify QIs, the median scores is used and the disagreement index, which is derived from the inter-percentile range corrected for symmetry. Ultimately, 17 QIs are determined to be appropriate after a three-stage process. Five of them described previously unseen subjects: protocolised care (the implementation of care and prevention management protocols), administration of low-density lipoprotein-cholesterol of ring medication, systematic evaluation of the patient's nutritional status, and integration of wound care speciality in the interdisciplinary team.

By evaluating the likelihood of DFU recurrence in elderly diabetic patients, Hong et al. [32] hoped to enhance both therapeutic and prophylactic measures. The goal is to construct accurate prediction models that assess the probability of DFU recurrence in older diabetic patients by taking into account high-risk factors such age, blood sugar management, alcohol usage, and smoking. Machine learning models are constructed utilising data collected from 138 elderly diabetic patients after data cleansing, screening for outliers, and feature integration. Using Support Vector Machines (SVM) are able to achieve an accuracy rate of 93%. Experimental research demonstrating the efficacy of SVM in predicting the recurrence risk of DFUs in elderly diabetic patients has provided clinical practitioners with a more trustworthy assessment tool. In particular, the study highlights the significance of machine learning for predicting the probability of recurrence in the treatment of diabetic foot ulcers in older persons. This technique offers medical solutions supported by computers for the management of diabetes in the elderly, allows for rapid intervention, and reduces the likelihood of recurrence.

In their attempt to assess the efficacy of ChatGPT and similar AI chatbots in providing data regarding DFUs, Shiraishi et al. [33] relied on previously established

criteria. Seven AI chatbots are evaluated by asking clinical questions (CQs) that are based on the DFU criteria. Additionally, the chatbots' reference accuracy was verified. Although there are variations in the level of evidence and recommendation grade, the average accuracy rate of the AI chatbots in ring CQs was 91.2%. Claude-2 outperformed the other chatbots with 99.6% of its references confirmed, while ChatGPT had the proportion of reference authenticity at 66.3%. This study demonstrates the potential of artificial intelligence chatbots as tools for medical knowledge dissemination and their accuracy in addressing clinical question types relevant to DFU. Careful use and further refinement are required for medical applications due to concerns such as AI hallucinations and the unpredictable accuracy of these chatbots. This study highlights the importance of enhancing these tools for efficient usage in patient education and clinical decision-making, as well as the ways in which AI is transforming the healthcare business.

Using a combination of a convolutional neural network (CNN) and a Swin Transformer architecture, MG et al. [34] presented a deep learning model for infection classification in DFU images. The objective is to improve detection accuracy using end-to-end mapping without prior information by integrating global and local feature extraction. The proposed model makes use of a combination of a Convolutional Neural Network (CNN) and a Swin Transformer. With the use of the Grad CAM method, we can see how the CNN and Transformer blocks make decisions. The DFUC Challenge dataset is used for both training and evaluation, showcasing the model's accuracy in classifying DFU images as infected or not. Accuracy (96.52%), specificity (97.08%), sensitivity (95.08%), and Matthews Correlation Coefficient (0.93) are excellent performance measures achieved by the model. The results show that the model can quickly identify DFU infections, which is promising for its future usage in healthcare. In difficult cases, the hybrid CNN and Swin Transformer architecture effectively combines the strengths of both models to correctly identify infected or non-infected DFU images. With the insights it provides into the model's decision-making process, Grad CAM aids in the localisation of sick areas in DFU photos. Clinical evaluation and management of DFU infections could be enhanced utilising this technique.

After utilising medical digital image processing to reconstruct the 3D model of blood vessels, Wu et al. [35] utilised this data, together with the original data's non-calcified blood vessel part, as training material for deep learning (DL). Their idea for a better model to identify small targets in vascular stenosis was based on YOLOv5. In order to enhance the identification of three distinct stenosis targets (I: <50%, II: 51% −99%, and III: entirely occluded), they substituted the Path Aggregation Network (PANET) with the Bidirectional Feature Pyramid Network (BiFPN), enhanced the backbone with the Convolutional Block Attention Module (CBAM), and swapped out C3 in the neck for GhostC3. For faster reasoning and convergence, they upgraded the Complete-IoU (CIoU) loss function to Alpha-Scylla-IoU (ASIoU) loss. Additionally, they opted for K-Means++ over K-Means to enhance algorithm convergence performance. Lastly, they benchmarked approach against five other popular models. With a mean Average Precision (mAP) of 85.40% and 74.60 FPS, this method was the most effective in detecting three different kinds of stenosis in diabetic feet, demonstrating the viability of utilising DL for this purpose.

3 Proposed Methodology

In this section, the proposed methodology is used to segment the DFU from the input images that is graphically shown in Fig. 1 and each of the block is explained in detailed.

The dataset was captured using two infrared cameras, the FLIR E60 and FLIR E6. Both cameras were configured to a standard resolution for capturing plantar thermograms, ensuring consistency across the dataset.

The cameras used identical operational conditions, including placement 1 m from the subject's feet and operation within a controlled temperature environment (20 ± 1°C). This ensured uniform data acquisition.

The setup included an IR-obstructing material applied to areas outside the plantar region to prevent thermal interference from other body parts. The data collection focused on capturing natural thermal emission from the plantar surface under a resting condition, avoiding external heating or cooling sources.

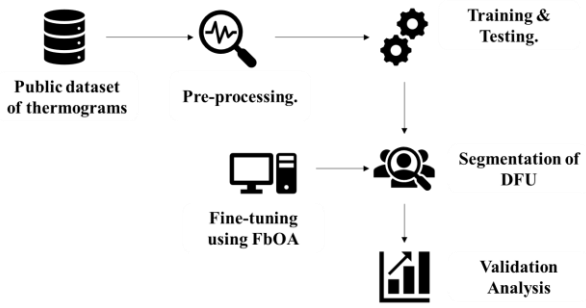

Fig. 1 Workflow of the proposed model.

3.1 Dataset Description and Augmentation

This study utilises a publicly available dataset consisting of thermograms [36]. Included in this data set are 334 plantar thermograms taken from 122 people with a diabetes mellitus (DM) diagnosis and 45 healthy controls. Sixteen women and twenty-nine men, ranging in age from 25 to 35, made up the DM group. There are 89 females and 33 males in the control group, and their ages ranged from 45 to 65. The participants are scouted from Puebla, Mexico, and their thermograms are taken over the course of 3 years (2012−2014). See Fig. 2 for an example of a pair of feet from each category [37].

The dataset comprises 334 plantar thermograms, with 122 thermograms from diabetic patients and 45 from healthy controls. The diabetic group includes individuals aged 25–35, with a gender distribution of 16 women and

29 men. The healthy control group comprises participants aged 45–65, with 89 females and 33 males. Exclusion criteria were applied to ensure data quality, eliminating patients with unrelated foot conditions or insufficient thermographic records. While comorbidities were not explicitly recorded, this remains a limitation of the study and a focus for future enhancement. These rigorous inclusion and exclusion criteria ensure the dataset's reliability for analyzing diabetic foot conditions. Four more pictures depicting plantar angiosomes are included in every thermogram. In this study, those are referred to as patches. Fig. 3 shows an example of both full-image and matching patch images (plantar angiosomes) from both groups. An infrared (IR) camera was placed 1m away from the subject's feet as they slept on a bed in order to acquire these images [37]. An IR obstructing substance was applied so that the temperature could not be detected from other parts of the body. At a temperature of 20 ± 1 ºC, 2 infrared cameras, the FLIR E60 and the FLIR E6, are employed [37]. The segmented foot and patch RGB images are utilised without pre-processing since they are already part of the database. Nevertheless, data augmentation is employed to both enlarge the dataset and achieve class parity. The process of augmentation involves flipping the photos horizontally or vertically, or both at the same time, as well as rotating them at 90º, 180º, or 270º. For image-level augmentation, 500 samples are made for every class, and for patch-level augmentation, 1500 samples are made for every class. Tabulated in Table 1 is the thermogram data broken down by class.

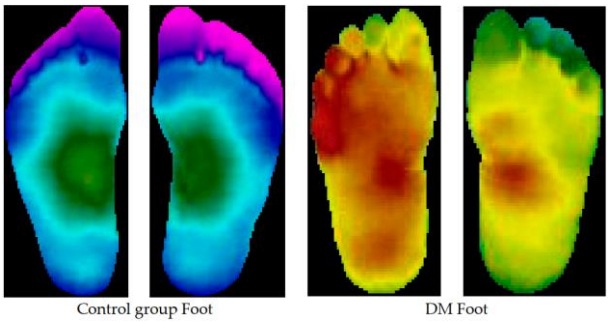

Fig. 2 Sample images of healthy foot and DM foot [37]. Reprinted under the Creative Common CC BY license from Ref. [37].

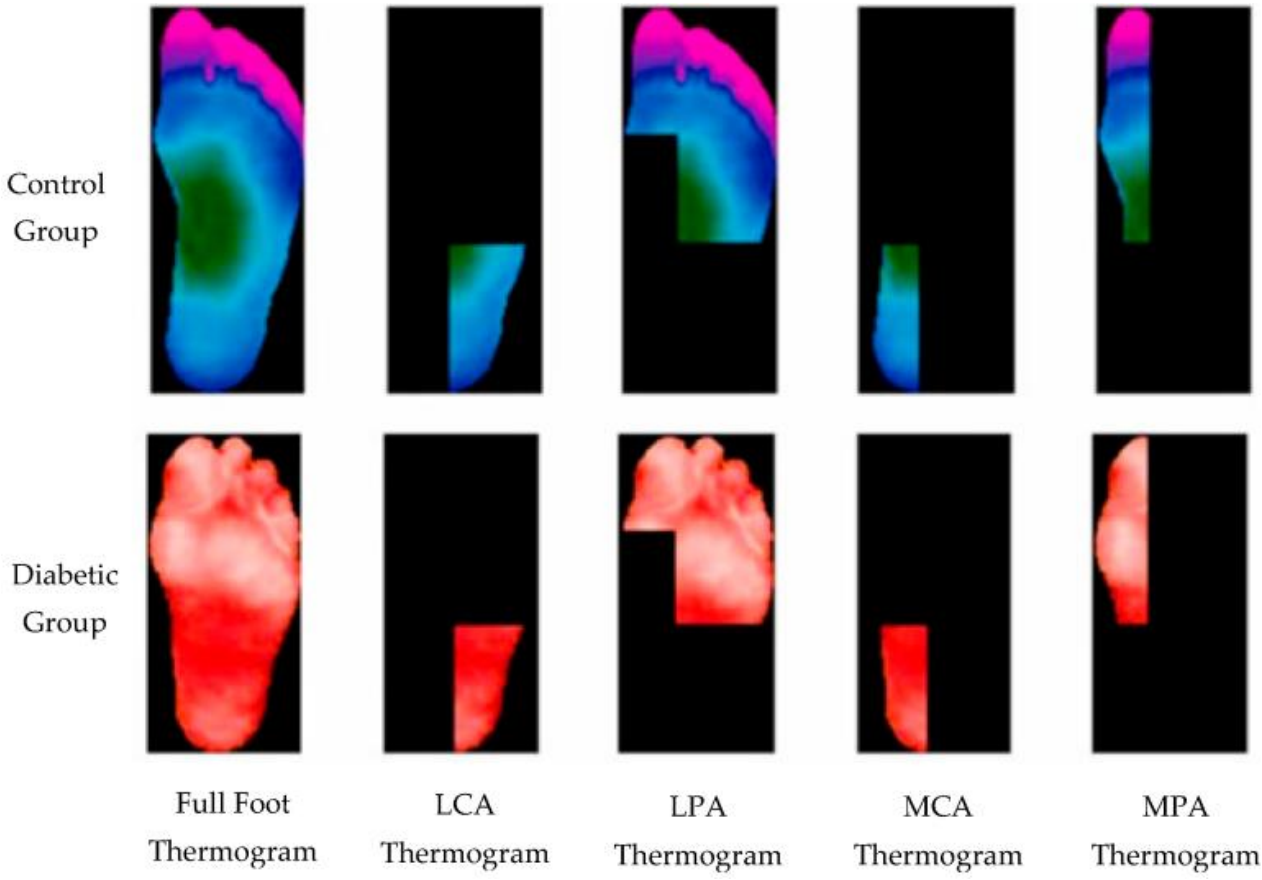

Fig. 3 Patch pictures (plantar angiosomes) and thermograms (for both the diabetes and control groups) are shown below. LCA stands for lateral calcaneal artery, LPA for lateral plantar artery, MCA for medial calcaneal artery, MPA for medial plantar artery, and so on [37]. Reprinted under the Creative Common CC BY license from Ref. [37].

Table 1 Thermogram image data detail: original and after augmentation.

Category	Diabetic Group	Control Group	Total
No. of cases	122	45	167
Original full images	244	90	334
Images after augmentation	500	500	1000
Original patches	976	360	1336
Patches after augmentation	1500	1500	3000

3.2 Segmentation Method

The research builds its model on diffusion models, which are generative models with two stages − a forward diffusion stage and a reverse diffusion stage − to extract the illness region from the input photos. Over the course of T iterations, the forward process corrupts a segmentation label x_0 with Gaussian noise. By turning the noising process backwards, the initial data can be recovered by training a neural network. One way to depict this is as:

$$p_\theta(x_{0:T-1}|x_T) = \prod_{t=1}^{T} p_\theta(x_{t-1}|x_t), \quad (1)$$

where θ is parameters for the reverse process. Starting from a Gaussian noise distribution, $p_\theta(x_T) = N(x_T;\, 0, I_{n\times n})$, where I is the original duplicate, the reverse process transforms the latent variable distribution $p_\theta(x_T)$ to the data distribution $p_\theta(x_0)$. The reverse process is symmetrical with respect to the forward process since it recovers the noisy image in stages to achieve the final, clear segmentation.

We use a UNet as our learning network to follow the typical DPM implementation. We used the raw image previously to condition the step estimate function ϵ in order to do the segmentation:

$$\epsilon_\theta(x_t, I, t) = D\big((E_t^I + E_t^x, t), t\big), \quad (2)$$

where E_t^I is the conditional feature embedding of the raw image, E_t^x at this stage is the segmentation map's feature embedding. In order to reconstruct, these 2 embeddings are combined and sent through a UNet decoder D. Along with the new embedding and decoding capabilities, the step index t is also included.

3.2.1 Dynamic Conditional Encoding

The conditional prior in the majority of conditional DPM implementations is an embedding of unique features. Nevertheless, ambiguous items are notoriously difficult to handle in medical picture segmentation, making it impossible to differentiate between the backdrop and lesions or tissues. Image modalities with low contrast increase this problem. Our proposed solution involves using a Dynamic Conditional Encoding at each stage to fix this issue. While the raw image does include precise segmentation target information, it has a difficult time differentiating itself from the background. The current-step segmentation map, however, does include improved target areas, though it is far from accurate. We are therefore inspired to incorporate the segmentation information from the current phase into the conditional raw picture encoding in order to achieve mutual complement. Integration is implemented at the feature level in particular. To improve the raw image encoder's intermediate feature, it is necessary to enable the features of the current-step encoding. The conditional feature map scales encoding features (m_I^k, m_x^k), where k is the layer index, are fused together to form a common shape. An attentive-like mechanism, A is used to accomplish the fusion. To create an affinity map using this method, it is need to normalise both feature maps using a layer and then multiply them. To further improve the attentive region, it is need to multiply the affinity map with the condition encoding features. Here is how it works:

$$\mathcal{A}(m_I^k, m_x^k) = \Big(LN(m_I^k) \otimes LN(m_x^k)\Big) \otimes m_I^k, \quad (3)$$

where $\otimes$ denotes element-wise multiplication, and LN denotes layer normalization. Both of the intermediate stages, which are convolutional stages built according to ResNet34, undergo this process.

The model is able to calibrate and localise itself in real-time with the use of this Dynamic Conditional Encoding technique. The incorporation of the noise-corrupted x_t embedding, however, might bring in extra high-frequency noise. In order to tackle this problem, the study suggests using the FF-Parser to limit the features' high-frequency components.

3.2.2 FF-Parser

The study uses FF-Parser as part of the feature integration pathway to fix the problem of high frequency noise caused by x_t embedding integration. The purpose of FF-Parser is to limit the x_t features that are associated with noise. Acquiring a parameterised attentive map for use with Fourier-space characteristics is the central concept. To initiate the process, we apply a 2D fast Fourier transform (FFT) to each spatial dimension of a decoder feature map $F[m] \in R^{H\times W\times C}$, which can be expressed as:

$$M = F[m] \in R^{H\times W\times C}, \quad (4)$$

where $F[\cdot]$ denotes the 2D FFT. Next, we modulate the spectrum of m by multiplying a parameterized attentive map $A \in C^{H\times W\times C}$ to M:

$$M' = A \otimes M, \quad (5)$$

where $\otimes$ signifies the product of elements. The last step is to use inverse FFT to return M′ to the spatial domain:

$$m' = \mathcal{F}^{-1}[M']. \quad (6)$$

A frequency filter is a common tool in digital image processing; FF-Parser is like a learnable version of it. While spatial attention focusses on individual frequencies, FF-Parser modifies their components on a global scale. As a result, it is trainable to limit adaptive integration's high-frequency components.

3.2.3 Training and Architecture

The training procedure for the proposed model adheres to the DPM standard. To be more precise, the loss can be expressed as:

$$\mathcal{L} = E_{x_{0,\epsilon,t}}\left[\left\|\epsilon - \epsilon_0\left(\sqrt{\hat{x}_t x_0} + \sqrt{1-}\,\hat{x}_t\epsilon, I_i, t\right)\right\|^2\right]. \quad (7)$$

In each iteration, a random pair of raw images I_i and segmentation label S_i is sampled for training. The iteration sum is sampled from a uniform distribution, besides ϵ is sampled from a Gaussian distribution.

Using a ResNet encoder and a UNet decoder, we can construct a modified ResUNet, which forms the core architecture of the suggested model. Two separate encoders are used to encode I and x_t. There are several residual blocks in each encoder's convolution stages. Each stage's number of residual blocks is based on ResNet34's. The two convolutional blocks that make up each residual block are as follows: a group-normalization layer, a SiLU activation layer, and finally, a convolutional layer. After passing through a linear layer, a SiLU activation, and still another linear layer, the time embedding reaches the residual block. After that, the output of the initial convolutional block is supplemented with the result. The final step of the encoding process involves adding the E^I and E^{x_t} that have been obtained. In order to forecast the end segmentation outcome, a conventional convolutional decoder is linked.

3.2.4 Fine-Tuning Using Football Optimizer

In this research, the learning parameters of the proposed segmentation model are optimally tuned using the Football Optimizer (FbOA) [38], as elaborated here. A comprehensive experimental setup is designed to evaluate the performance and effectiveness of the proposed FbOA. The objective is to assess the algorithm's exploration and exploitation capabilities and its ability to avoid local optima. The implementation includes an in-depth analysis of the algorithm's exploration and exploitation benchmarks, incorporating elements such as dynamic decision-making and ball-passing strategies inspired by football tactics. This process employs various mathematical equations and update procedures that simulate the strategic approaches used by football players, ensuring a balanced exploration and exploitation of productive zones within the solution space. The following sub-sections provide a detailed discussion of these aspects, beginning with the algorithm's exploration performance.

3.2.4.1 Exploration Performance

In the FbOA, exploration performance is based on the assumption that in every football pass, one of the players performs his pass with a certain speed velocity. This speed variation is important to balance the exploration of the search space and exploitation of the existing regions to avoid getting trapped in the local optimum.

To model this dynamic process, the next stage of the algorithm, represented by $Fb(S(t+1))$, is defined as:

$$Fb(S(t+1)) = i, \quad (8)$$

where $Fb(S(t+1))$ denotes the updated state or solution at the next iteration t + 1, i represents the player as the agent involved in the optimization process, contributing to the variation in exploration.

Football Velocity

The Eq. (9) represents the velocity of each player (or agent):

$$V_n = F_{max}\left(b_x.a_i[F_{ext} - F_{min}] + r.b_y.a_j[F_{best} - F_{min}] \times cos\left(\frac{\pi}{Iteration}\right)\right), \quad (9)$$

where V_n is the velocity of the player (agent) at iteration n, F_{max} is the maximum force applied, representing the upper limit of velocity, b_x and b_y are coefficients determining the influence of different directions in the search space, a_i and a_j are acceleration factors impacting the speed adjustments, F_{ext} represents the external force or influence in the optimization context, F_{min} is the minimum force, indicating the lower bound of velocity, F_{best} is the best force or position found so far in the optimization process, r is a random factor introducing variability and enhancing exploration, $cos\left(\frac{\pi}{Iteration}\right)$ modulates the velocity based on the number of iterations to balance exploitation.

The equation captures the dynamic nature of exploration by allowing agents to adapt their velocities, thus effectively covering a broader search space.

Update for Best Force

To further refine the exploration process, the best force is updated using the following Eq. (10):

$$F_{best} = \frac{1}{K}\sum_{n=0}^{K}\left(\frac{F_{max}^{n^2}}{(2n+1)^2}\right), \quad (10)$$

where F_{best} represents the best position or force in the current optimization context, K is an exponential factor that increases from 0 to 1 throughout the iterations, balancing between exploration and exploitation, F_max is raised to the power of n^2, which intensifies the search focus on promising regions as the iterations proceed,

$(2n + 1)^2$ is a normalization term to control the update rate.

By continuously adjusting the velocities and updating the best force, FbOA enhances its ability to explore the solution space thoroughly while adapting to the iterations.

3.2.4.2 Exploitation Performance

The tuning aspect of the FbOA in exploitation is centered on enhancing the solutions within the specified search space to get the best or nearly the best solutions. The exploitation mechanism is meant to further focus on the more rewarding areas during the exploration. The update rule for adjusting the position of an agent in the exploitation phase is given by:

$$Fb(S(t+1)) = F_i + z_3 \cdot Fb(S(t)) + K \cdot sin\left(\frac{\pi}{Iteration}\right), \quad (11)$$

where $Fb(S(t+1))$ is the updated solution or position at the next iteration $t + 1$, F_i represents the current position or force influencing the aggrandisement, z_3 is a control parameter that adjusts the balance between the current and the new position, $Fb(S(t))$ is the current state or position at iteration t, K is an exponential factor that increases throughout the iterations, gradually shifting focus from exploration to exploitation, $sin\left(\frac{\pi}{Iteration}\right)$ introduces a sinusoidal modulation to enhance the convergence speed toward the optimal solution.

This update mechanism helps FbOA take advantage of the solution space and ensures that FbOA converges on precise solutions during the iterations.

Mutation

To avoid this, the Football Optimization Algorithm used in this study incorporates a mutation strategy that introduces variability into the search process, in which the algorithm initially converges with local optima. Through the mutation mechanism, the site of the agents changes constantly in the search space, thus making a transition and avoiding being trapped in an area with poor solutions. The mutation is defined by:

$$S(t) = \left(K \cdot a_q\left(\frac{2n+1}{x}\right) + K \cdot cos\left(\frac{\pi}{Iteration}\right)\right), \quad (12)$$

where $S(t)$ represents the mutated solution at iteration t, K is an exponential factor influencing the extent of mutation, a_q is a factor that scales the mutation magnitude based on the current solution, $\frac{2n+1}{x}$ acts as a normalization term to control the mutation effect, $cos\left(\frac{\pi}{Iteration}\right)$ modulates the mutation with a cosine function to introduce randomness and diversity in the search, iteration represents the current iteration number.

By incorporating this mutation strategy, FbOA can search distant solution areas and thus avoid local optima in the optimization framework, resulting in higher performance and robustness of the algorithm. Table 2 displays the initial parameter values used in this study for all the algorithms: population size, sum of iterations and independent runs. All these general parameters are set for all the algorithms with no exception. Additionally, specific parameters for the Feedback-based Optimization Algorithm (FbOA) are detailed, such as the ranges for constants a_1, a_2, b_1, b_2, and other control variables like r_1, z, Θ, and a, which influence the behaviour of the algorithm.

Table 2 Initial parameters of algorithms.

Algorithm	Parameter	Value
All algorithms	Population size	30
	Sum of iterations	500
	Number of runs	30
FbOA	a_1	[0, 1]
	a_2	[0, 1]
	b_1	[0, 1]
	b_2	[0, 1]
	r_1	[0, 2]
	z	[0, 2]
	Θ	[0, 12π]
	a	[-8, 8]

4 Results and Discussion

The PyTorch platform was used to implement all experiments, and four Tesla P40 GPUs with 24GB of RAM are used for training and testing [39]. The dimensions of all the photographs are adjusted to 256 × 256 pixels. With the help of the FbOA optimiser, the networks are trained end-to-end. The rate was set to 10^{-4} besides the batch size was 32 when the model was trained [40].

4.1 Validation Analysis of Input Data

Here, 3 set of input data is used to test the effectiveness of the projected model that is shown in Table 3.

4.2 Validation Analysis of Training and Testing Ratio Data

Fig. 4 mentions the efficiency of the proposed prototypical based on training and testing data variations in terms of different metrics.

The proposed model's performance was assessed across different data split ratios (80−20%, 70−30%, and 60−40%) to examine its effectiveness in training and testing scenarios. For an 80−20% split, the model accomplished a high training accuracy of 0.98 and a test accuracy of 0.92, with an AUC of 0.92, precision at 0.93, recall and F_1-score both at 0.92, and a specificity of 0.98, indicating balanced sensitivity and specificity.

Table 3 Validation analysis based on input types.

Parameters	Input data	MPA	Mean Intersection over Union (MioU)	Running Time
86 M	Image level	0.8331	0.7058	2.67 s/item
307 M	Patch level	0.8313	0.7151	4.07 s/item
632 M	Combined	0.8376	0.7185	4.2 s/item

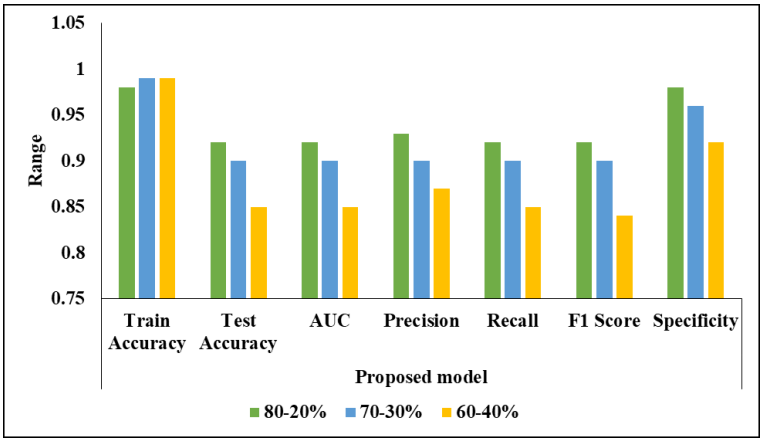

Fig. 4 Graphical description of proposed model.

In the 70−30% split, the model demonstrated a slightly higher train accuracy of 0.99 and a test accuracy of 0.90, with AUC, precision, recall, and F_1-score all at 0.90, and a specificity of 0.96, showcasing consistent performance despite a larger test set. For the 60−40% split, the model maintained a high train accuracy of 0.99 but experienced a slight drop in test accuracy to 0.85. Its AUC, recall, and F_1-score stood at 0.85, while precision was 0.87 and specificity was 0.92, reflecting the impact of reduced training data. Overall, the proposed model displayed robust accuracy and balanced metrics across varying data splits, demonstrating its adaptability and effectiveness in different training and testing conditions.

4.3 Validation Analysis of Input Batch Size

Table 4 presents the validation analysis of proposed model by changing its batch sizes in terms of different metrics.

The experimental analysis of the proposed model across different batch sizes (4, 8, 16, and 32) highlights its performance in training besides testing accuracy, AUC, precision, recall, F_1-score, and specificity. For batch sizes of 4 and 8, the model achieved perfect test accuracy of 1.00, with all evaluative metrics (AUC, precision, recall, F_1-score, and specificity) at 1.00, indicating optimal model performance and consistency in both training and testing phases. At a batch size of 16, although the model reached full training accuracy (1.00), the test accuracy and all other metrics dropped significantly to 0.50, reflecting underperformance likely due to batch size inefficiencies. Similarly, for a batch size of 32, while training accuracy remained perfect (1.00), the test accuracy and other evaluative metrics are moderate at 0.75. This comparison indicates that smaller batch sizes (4 and 8) provided the best performance consistency, while larger batch sizes resulted in reduced generalization, as observed by lower test accuracy and evaluative scores.

4.4 Comparative Analysis: Segmentation Results

Table 5 and Fig. 4 provide the experimental analysis of projected model with existing techniques that are taken from the related work section. However, the existing models use different datasets for validation, the basic model is implemented by our considered dataset and results are averaged in this work.

The performance comparison of various methods, with Support Vector Machine (SVM), DNN, Deep Convolutional Neural Network (DCNN), ResNet50, MobileNetV2, HCNNet, FusionNet, and the proposed Op-DPS model, is summarized across key metrics: precision, recall, F_1-score, overall accuracy, besides IoU. The Op-DPS model demonstrates the highest precision at 0.8955 and recall at 0.8553, resulting in an F_1-score of 0.8750, indicating its superior capability to balance precision and recall effectively. Additionally, it achieves an overall accuracy of 0.9927 and an IoU of 0.8896, reflecting exceptional performance in accurately classifying instances. In comparison, FusionNet follows closely with an F_1-score of 0.8678 and an overall accuracy of 0.9807, while the remaining methods show lower metrics across the board, with DNN recording the lowest F_1-score of 0.7995 besides an IoU of 0.8476. Overall, the results highlight the Op-DPS model as the most effective approach among those evaluated, excelling in all critical performance indicators.

Table 4 Experimental Analysis of proposed model on various batch size.

Batch Size	Test accuracy	AUC	Precision	Recall	F_1-score	Train accuracy	Specificity
4	1.00	1.00	1.00	1.00	1.00	0.98	1.00
8	1.00	1.00	1.00	1.00	1.00	0.98	1.00
16	0.50	0.50	0.50	0.50	0.50	1.00	0.50
32	0.75	0.75	0.75	0.75	0.75	1.00	0.75

Table 5 Comparative analysis of various algorithms.

Method	Precision	Recall	F_1-score	Overall Accuracy	IoU
SVM [32]	0.8639	0.8178	0.8402	0.9780	0.8505
DNN [21]	0.8891	0.7264	0.7995	0.9742	0.8476
DCNN [25]	0.8343	0.7367	0.7825	0.9710	0.8061
ResNet50 [22]	0.8827	0.7944	0.8363	0.9780	0.8477
MobileNetV2 [24]	0.8848	0.8139	0.8479	0.9793	0.8570
HCNNet [27]	0.8758	0.8367	0.8558	0.9801	0.8634
FusionNet [29]	0.8856	0.8231	0.8678	0.9807	0.8652
Op-DPS	0.8955	0.8553	0.8750	0.9927	0.8896

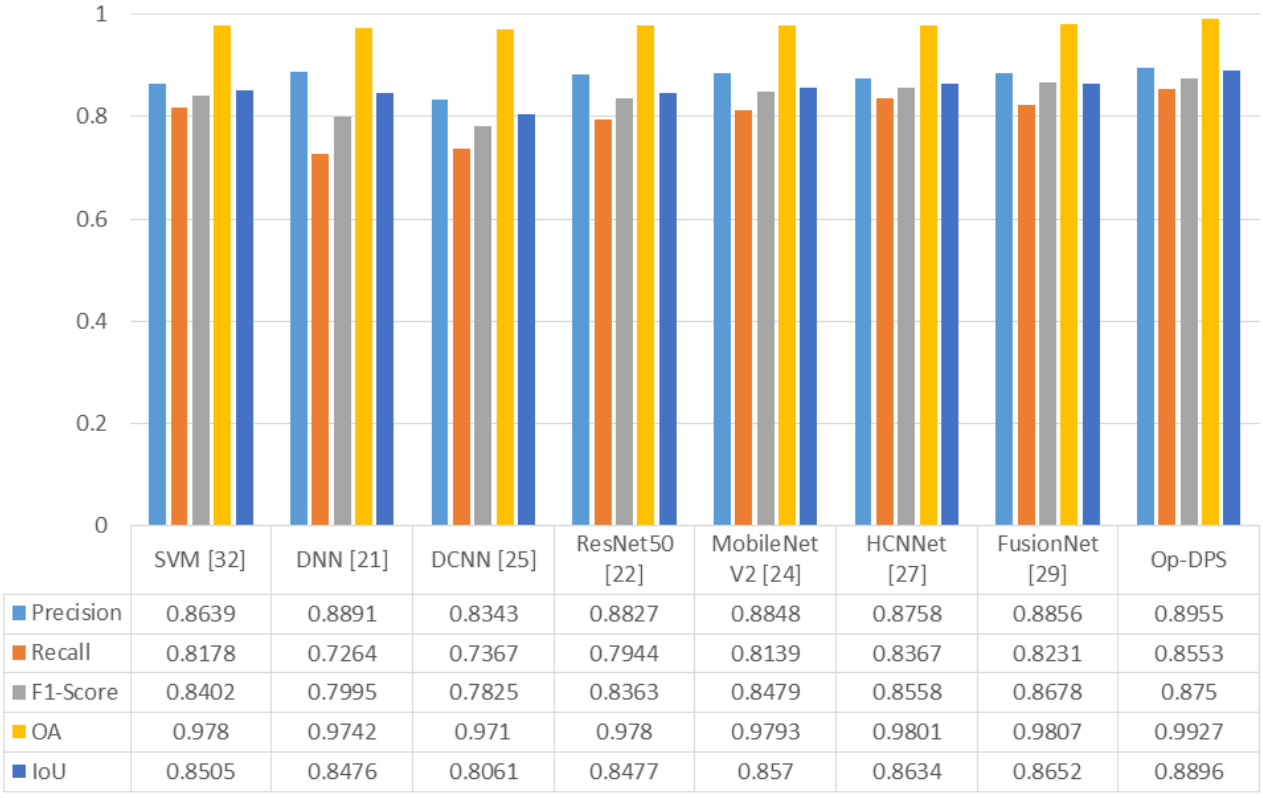

Fig. 5 Graphical Description of proposed model with existing models.

Baseline classification algorithms such as SVM, DNN, and ResNet50 were optimized using conventional techniques like grid search and random search. These techniques explored the parameter space by systematically evaluating combinations of hyperparameters, such as learning rate, regularization factors, and activation functions. In comparison, the proposed approach utilized the Football Optimization Algorithm (FbOA), which mimics football dynamics to optimize model parameters efficiently. FbOA's strategies, such as velocity adjustment and mutation, enable it to explore a larger solution space and avoid local optima, leading to superior parameter tuning. This difference in optimization techniques ensures the proposed model's performance is not underestimated relative to the baseline methods.

5 Conclusion

The segmentation of DFU foot is demonstrated in this paper by means of a thorough and comparative examination of deep-learning and machine-learning procedures. At the image, patch, and combined image-patch levels, the thermogram data of both DFU besides non-DFU foot are utilised. Image segmentation system Op-DPS is introduced in this paper. It improves segmentation performance by combining 2 unique techniques: FF-Parser and Dynamic Conditional Encoding. Results showed that FbOA converged more quickly, solved the problem accurately, and was more robust when used to fine-tune the parameters of the suggested model. An algorithm that optimises a search space by minimising the chances of getting stuck by local optimality through high exploration and low exploitation incorporates many football techniques. To show the outcomes of the machine-learning methods we used a number of thermogram characteristics. From the various machine-learning approaches, the suggested model emerged victorious. The suggested deep-learning model outperformed both the pre-trained and competing models. Using the thermogram data, comparing the suggested model to an existing solution was not easy. Nevertheless, when looking at the 2 models at a more abstract level, the suggested model outperformed the others considering the limitations.

Data Availability Statement

The dataset considered in this work are taken from publicly available site, which is referred in Refs. [36−37].

Conflict of Interest

Author declares there is no conflict of interest.

Acknowledgment

We thank all the staff of our institution for their cooperation and kind support throughout the course of our research.

Funding Statement

Author declares there is no funding are provided for this work.

References

1. C. C. Kendrick, B. Cassidy, J. M. Pappachan, C. O'Shea, C. J. Fernandez, E. Chacko, K. Jacob, N. D. Reeves, and M. H. Yap, "Translating Clinical Delineation of Diabetic Foot Ulcers into Machine Interpretable Segmentation," in Diabetic Foot Ulcers Grand Challenge, M. H. Yap, C. Kendrick, and R. Brüngel (Eds.), Springer Nature Switzerland, 15335 (2025).
2. A. Mahbod, G. Schaefer, R. Ecker, and I. Ellinger, "Automatic foot ulcer segmentation using an ensemble of convolutional neural networks," in 26th International Conference on Pattern Recognition (ICPR), IEEE, 4358−4364 (2021).
3. R. V. Prakash, K. S. Kumar, "Development of automatic segmentation techniques using convolutional neural networks to differentiate diabetic foot ulcers," International Journal of Advanced Computer Science and Applications 13(11), (2022).
4. J. Reyes-Luévano, J. A. Guerrero-Viramontes, J. Rubén Romo-Andrade, and M. Funes-Gallanzi, "DFU_VIRNet: A novel Visible-InfraRed CNN to improve diabetic foot ulcer classification and early detection of ulcer risk zones," Biomedical Signal Processing and Control 86, 105341 (2023).
5. D. Kucharski, A. Kostuch, F. Noworolnik, A. Brodzicki, and J. Jaworek-Korjakowska, "DFU-Ens: End-to-End diabetic foot ulcer segmentation framework with vision transformer based detection," in Diabetic Foot Ulcers Grand Challenge, M. H. Yap, C. Kendrick, and B. Cassidy (Eds.), Springer International Publishing, 13797, 101–112 (2023).
6. T.-Y. Liao, C.-H. Yang, Y.-W. Lo, K.-Y. Lai, P.-H. Shen, and Y.-L. Lin, "HarDNet-DFUS: enhancing backbone and decoder of HarDNet-MSEG for diabetic foot ulcer image segmentation," in Diabetic Foot Ulcers Grand Challenge, M. H. Yap, C. Kendrick, and B. Cassidy (Eds.), Springer International Publishing, 13797, 21–30 (2023).
7. H.-N. Huang, T. Zhang, C.-T. Yang, Y.-J. Sheen, H.-M. Chen, C.-J. Chen, and M.-W. Tseng, "Image segmentation using transfer learning and Fast R-CNN for diabetic foot wound treatments," Frontiers in Public Health 10, 969846 (2022).

8. A. Kairys, R. Pauliukiene, V. Raudonis, and J. Ceponis, "Towards home-based diabetic foot ulcer monitoring: a systematic review," Sensors 23(7), 3618 (2023).
9. B. Gunapriya, T. Rajesh, A. Thirumalraj, and B. Manjunatha, "LW-CNN-based extraction with optimized encoder-decoder model for detection of diabetic retinopathy," Journal of Autonomous Intelligence 7(3), (2023).
10. H. J. Chae, S. Lee, H. Son, S. Han, and T. Lim, "Generating 3D bio-printable patches using wound segmentation and reconstruction to treat diabetic foot ulcers," Proceedings of the IEEE/CVF Conference on Computer Vision and Pattern Recognition 2539–2549 (2022).
11. D. Bouallal, H. Douzi, and R. Harba, "Diabetic foot thermal image segmentation using Double Encoder-ResUnet (DE-ResUnet)," Journal of Medical Engineering & Technology 46(5), 378–392 (2022).
12. H. Yi, W. Xu, Z. Jiang, J. Gao, Q. Kang, Q. Lao, and K. Li, "OCRNet for diabetic foot ulcer segmentation combined with edge loss," Diabetic Foot Ulcers Grand Challenge 13797, 31–39 (2023).
13. M. Hassib, M. Ali, A. Mohamed, M. Torki, and M. Hussein, "Diabetic foot ulcer segmentation using convolutional and transformer-based models," in Diabetic Foot Ulcers Grand Challenge, M. H. Yap, C. Kendrick, and B. Cassidy (Eds.), Springer International Publishing, 13797, 83–91 (2023).
14. A. Kairys, V. Raudonis, "Analysis of training data augmentation for diabetic foot ulcer semantic segmentation," Electronics 12(22), 4624 (2023).
15. P. Xu, X. Wu, Y. Li, E. U. Haq, J. Yin, and K. Li, "Ensemble learning for diabetic foot ulcer segmentation based on DFUC2022 dataset," Proceedings of the 2022 6th International Conference on Electronic Information Technology and Computer Engineering, 1750–1754 (2022).
16. R. Brüngel, S. Koitka, and C. M. Friedrich, "Unconditionally generated and pseudo-labeled synthetic images for diabetic foot ulcer segmentation dataset extension," in Diabetic Foot Ulcers Grand Challenge, M. H. Yap, C. Kendrick, and B. Cassidy (Eds.), Springer International Publishing, 13797, 65–79 (2023).
17. J. Zhang, Y. Qiu, L. Peng, Q. Zhou, Z. Wang, and M. Qi, "A comprehensive review of methods based on deep learning for diabetes-related foot ulcers," Frontiers in Endocrinology 13, 945020 (2022).
18. G. Scebba, J. Zhang, S. Catanzaro, C. Mihai, O. Distler, M. Berli, and W. Karlen, "Detect-and-segment: A deep learning approach to automate wound image segmentation," Informatics in Medicine Unlocked 29, 100884 (2022).
19. C. Cao, Y. Qiu, Z. Wang, J. Ou, J. Wang, A. H. Hounye, M. Hou, Q. Zhou, and J. Zhang, "Nested segmentation and multi-level classification of diabetic foot ulcer based on mask R-CNN," Multimedia Tools and Applications 82(12), 18887–18906 (2023).
20. J. P., S. K. B. K., and S. Jayaraman, "Automatic foot ulcer segmentation using conditional generative adversarial network (AFSegGAN): A wound management system," PLOS Digit Health 2(11), e0000344 (2023).
21. R. Sarmun, M. E. H. Chowdhury, M. Murugappan, A. Aqel, M. Ezzuddin, S. M. Rahman, A. Khandakar, S. Akter, R. Alfkey, and A. Hasan, "Diabetic foot ulcer detection: combining deep learning models for improved localization," Cognitive Computation 16(3), 1413–1431 (2024).
22. A. M. El-Kady, M. M. Abbassy, H. H. Ali, and M. F. Ali, "Advancing diabetic foot ulcer detection based on resnet and gan integration," Journal of Theoretical and Applied Information Technology 102(6), 2258–2268 (2024).
23. R. Basiri, K. Manji, P. M. LeLievre, J. Toole, F. Kim, S. S. Khan, and M. R. Popovic, "Protocol for metadata and image collection at diabetic foot ulcer clinics: enabling research in wound analytics and deep learning," BioMedical Engineering OnLine 23(1), 12 (2024).
24. S. Biswas, R. Mostafiz, B. K. Paul, K. M. M. Uddin, Md. A. Hadi, and F. Khanom, "DFU_XAI: A deep learning-based approach to diabetic foot ulcer detection using feature explainability," Biomedical Materials & Devices 2(2), 1225–1245 (2024).
25. N. F. Almufadi, H. F. Alhasson, and S. S. Alharbi, "E-DFu-Net: An efficient deep convolutional neural network models for diabetic foot ulcer classification," Biomolecules and Biomedicine 25(2), 445–460 (2025).
26. C. Thota, D. Jackson Samuel, M. Musa Jaber, M. M. Kamruzzaman, R. V. Ravi, L. J. Gnanasigamani, and R. Premalatha, "Image smart segmentation analysis against diabetic foot ulcer using internet of things with virtual sensing," Big Data 12(2), 155–172 (2024).
27. S. K. Das, S. Namasudra, and A. K. Sangaiah, "HCNNet: hybrid convolution neural network for automatic identification of ischaemia in diabetic foot ulcer wounds," Multimedia Systems 30(1), 36 (2024).
28. M. K. Dhar, T. Zhang, Y. Patel, S. Gopalakrishnan, and Z. Yu, "FUSegNet: A deep convolutional neural network for foot ulcer segmentation," Biomedical Signal Processing and Control 92, 106057 (2024).
29. S. Biswas, R. Mostafiz, M. S. Uddin, and B. K. Paul, "XAI-FusionNet: Diabetic foot ulcer detection based on multi-scale feature fusion with explainable artificial intelligence," Heliyon 10(10), e31228 (2024).
30. N. Zhao, L. Yu, X. Fu, W. Dai, H. Han, J. Bai, J. Xu, J. Hu, and Q. Zhou, "Application of a Diabetic Foot Smart APP in the measurement of diabetic foot ulcers," International Journal of Orthopaedic and Trauma Nursing 54, 101095 (2024).
31. F. M. Lusendi, A.-S. Vanherwegen, F. Nobels, and G. A. Matricali, "A multidisciplinary Delphi consensus to define evidence-based quality indicators for diabetic foot ulcer care," European Journal of Public Health 34(2), 253–259 (2024).

32. S. Hong, Y. Chen, Y. Lin, X. Xie, G. Chen, H. Xie, and W. Lu, "Personalized prediction of diabetic foot ulcer recurrence in elderly individuals using machine learning paradigms," Technology and Health Care 32, 265–276 (2024).
33. M. Shiraishi, H. Lee, K. Kanayama, Y. Moriwaki, and M. Okazaki, "Appropriateness of artificial intelligence chatbots in diabetic foot ulcer management," The International Journal of Lower Extremity Wounds 15347346241236811 (2024).
34. M.G Sumithra, C. Venkatesan, "SwinDFU-Net: Deep learning transformer network for infection identification in diabetic foot ulcer," Technology and Health Care 33(1), 601–618 (2025).
35. C. Wu, C. Xu, S. Ou, X. Wu, J. Guo, Y. Qi, and S. Cai, "A novel approach for diabetic foot diagnosis: Deep learning-based detection of lower extremity arterial stenosis," Diabetes Research and Clinical Practice 207, 111032 (2024).
36. D. A. Hernandez-Contreras, H. Peregrina-Barreto, J. de J. Rangel-Magdaleno, and F. J. Renero-Carrillo, "Plantar thermogram database for the study of diabetic foot complications," IEEE Access 7, 161296–161307 (2019).
37. I. Khosa, A. Raza, M. Anjum, W. Ahmad, and S. Shahab, "Automatic diabetic foot ulcer recognition using multi-level thermographic image data," Diagnostics 13(16), 2637 (2023).
38. E.-S. M. El-Kenawy, F. H. Rizk, A. M. Zaki, M. E. Mohamed, A. Ibrahim, A. A. Abdelhamid, N. Khodadadi, E. M. Almetwally, and M. M. Eid, "Football Optimization Algorithm (FbOA): A novel metaheuristic inspired by team strategy dynamics," Journal of Artificial Intelligence and Metaheuristics 8(1), 21–38 (2024).
39. R. Aluvalu, T. Sharma, U. M. Viswanadhula, A. D. Thirumalraj, M. V. V. Prasad Kantipudi, and S. Mudrakola, "Komodo dragon mlipir algorithm-based CNN model for detection of illegal tree cutting in smart iot forest area," Recent Advances in Computer Science and Communications 17(6), e260124226370 (2024)
40. V. Uma Maheswari, S. Stephe, R. Aluvalu, A. Thirumalraj, and S. N. Mohanty, "Chaotic satin bowerbird optimizer based advanced ai techniques for detection of COVID-19 diseases from CT scans images," New Generation Computing 42(5), 1065–1087 (2024).